

See discussions, stats, and author profiles for this publication at: <https://www.researchgate.net/publication/51116116>

Size-Selective Template-Assisted Electrophoretic Assembly of Nanoparticles for Biosensing Applications

ARTICLE in LANGMUIR · JUNE 2011

Impact Factor: 4.46 · DOI: 10.1021/la104975u · Source: PubMed

CITATIONS

8

READS

49

7 AUTHORS, INCLUDING:



Sivasubramanian Somu

Northeastern University

78 PUBLICATIONS 577 CITATIONS

[SEE PROFILE](#)



Vladimir P Torchilin

Northeastern University

358 PUBLICATIONS 24,674 CITATIONS

[SEE PROFILE](#)



Ahmed A Busnaina

Northeastern University

213 PUBLICATIONS 1,704 CITATIONS

[SEE PROFILE](#)

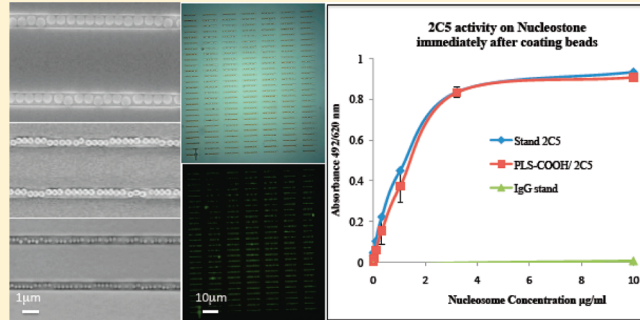
Size-Selective Template-Assisted Electrophoretic Assembly of Nanoparticles for Biosensing Applications

Salome Siavoshi,[†] Cihan Yilmaz,[†] Sivasubramanian Somu,[†] Tiziana Musacchio,[‡] Jaydev R. Upponi,[‡] Vladimir P. Torchilin,[‡] and Ahmed Busnaina^{*,†}

[†]NSF Nanoscale Science and Engineering Center for High-Rate Nanomanufacturing and [‡]Center for Pharmaceutical Biotechnology & Nanomedicine, Northeastern University, Boston, Massachusetts 02115, United States

 Supporting Information

ABSTRACT: The precise, size-selective assembly of nanoparticles gives rise to many applications where the assembly of nano building blocks with different biological or chemical functionalizations is necessary. We introduce a simple, fast, reproducible-directed assembly technique that enables a complete sorting of nanoparticles with single-particle resolution. Nanoparticles are size-selectively assembled into prefabricated via arrays using a sequential template-directed electrophoretic assembly method. Polystyrene latex (PSL) nanoparticles with diameters ranging from 200 to 50 nm are selectively assembled into vias comparable to nanoparticle diameter. We investigate the effects of particle size and via size on the sorting efficiency. We show that complete sorting can be achieved when the size of the vias is close to the diameter of the nanoparticles and the size distribution of the chosen nanoparticles does not overlap. The results also show that it is necessary to keep the electric field on during the insertion and removal of the template. To elucidate the versatility and nil effects that the electrophoresis assembly technique has on the assembled nanoparticle characteristics, we have assembled cancer-specific monoclonal antibody-2C5-coated nanoparticles and have also shown that they can successfully measure low concentrations of the nucleosome (NS) antigen.



INTRODUCTION

Ordered arrays of nanoparticles have attracted a tremendous amount of attention because of their potential applications in various emerging fields such as nanophotonic crystals, nanoelectronics, and nanosensors.^{1–7}

Because of their high surface area and size compatibility with biological elements such as enzymes, antigens, and antibodies, nanoparticles can carry on important functions such as the immobilization of biomolecules and the catalysis of electrochemical reactions. Unlike commercially available enzyme-linked immunosorbent assay (ELISA)⁸ sensors, it has been shown that employing uniformly distributed mAb-coated nanoparticles on the sensor surface increases the orientation and distribution of antibodies,^{9–11} thus increasing the antibody–antigen binding events and hence the sensitivity of the sensor. This makes the nanoparticles a strong candidate for fabricating biosensing devices.^{12–15} The simultaneous detection of multiple biomarkers has attracted tremendous interest in the field of microbiosensors.^{16–20} Nanoparticle-based sensors can potentially enable multiplex detection. To achieve multiple detection capability, particles with different diameters can be coated with different biomarker proteins and size-selectively assembled at the desired locations on surfaces. Also, the size-selective assembly of nanoparticles has potential applications in multiplexing the detection of vapor

sensors²¹ and miniaturizing nanoparticle-based chemical nose sensors,²² enabling *in vivo* detection. For these applications, precise and selective positioning of nanoparticles is challenging.

Methods for assembling nanoparticles suspended in a solution onto prefabricated patterns on a template can be broadly classified into self-assembly^{23–26} and directed assembly.^{27–29} Previous attempts to position nanoparticles on a template according to their size have been limited to template-assisted self-assembly (TASA) by controlling either the chemical properties^{30–34} or topography^{35–39} of the template. Topographically patterned substrates have been used as 3-D templates to guide crystalline colloidal assembly. Yin and Xia^{35,36,38} used patterned topography and capillary interactions to assemble monodisperse polystyrene particles into a variety of complex aggregates (such as polygonal and polyhedral clusters) that have well-controlled sizes, shapes, and structures, and their work has been recently reviewed.⁴⁰ Recently, Kuemin et al.³⁹ showed that it is possible to employ TASA to trap 200, 350 nm, and 500 nm particles on carefully designed topographic features. Relying only on the wetting of the particle suspension and employing a single evaporation/dip-coating step, Fan et al.^{30,41}

Received: December 16, 2010

Revised: April 28, 2011

Published: May 11, 2011

showed that particles of different size can be arranged in arrays from a single suspension onto patches well wet by the suspension. The particles in the suspension were placed on the patterned substrate and separated by size. Although smaller particles were deposited on small patches, larger particles as well as smaller particles were deposited on the larger patches. During dewetting, the smaller particles were moved by convection to the edge of the large patches forming a coffee ring, and thus even on the large patch there was size segregation. Despite the good yield, these assembly techniques relying on evaporation or dip-coating are slow, limiting the possibility of high-rate manufacturing. Therefore, a fast, high-yield technique appropriate to the size-selective assembly of nanoparticles of various kinds and surface functionalizations has not yet been demonstrated.

In this article, we present a template-assisted method with the application of an external electric field to size-selectively assemble nanoparticles over a large area in a short time. This process relies on the knowledge of the particle zeta potential impact on the electrophoretic phenomena, template feature size, and nanoparticle size to assemble them selectively into arrays. Particles are assembled sequentially from solutions containing only a single-sized particle. This is a reliable means of making size-sorted nanoparticle arrays from several single-sized nanoparticle solutions for subsequent use in various devices. In our sequential template-assisted assembly, particles are electrophoretically assembled into vias with various sizes generated on a PMMA/gold surface using electron beam lithography. The larger particles are assembled first to fill the larger vias; the remaining vias are then filled with smaller particles. With this technique, we can achieve a complete separation of particles on the basis of their size. We demonstrate that even functionalized mAb-2C5-coated particles can be assembled electrophoretically inside trenches without any deterioration of their characteristics. We also show that the resulting chip can successfully detect low concentrations of fluorescently tagged nucleosome (NS) antigen. Therefore, we suggest that the presented size-selective assembly technique can be promising for future nanoparticle-based multiplex miniaturized biosensing devices.

EXPERIMENTS

Template Fabrication. Six nanometer Cr/40 nm Au was sputtered onto a 380- μm -thick silicon substrate with 150 nm of thermally grown SiO_2 . Subsequently, a 150-nm-thick poly(methyl methacrylate) (PMMA) film was spin coated, followed by baking on a hot plate at a temperature of 100 °C for 90 s. The sample was then exposed to an electron beam to generate arrays of vias on the PMMA. The exposed PMMA film was developed in a methyl isobutyl ketone (MIBK)/isopropyl alcohol (IPA) (1:3) solution for 90 s, followed by rinsing in IPA and deionized (DI) water for 30 s and 5 min, respectively. The schematic of the template fabrication process is shown in Figure 1a. The template consists of arrays of vias with different diameters providing a platform for the selective assembly of differently sized particles.

Solution Preparation. Polystyrene latex (PSL) nanoparticle solution with an initial concentration of 1 wt % was diluted 200-fold in DI water. NH_4OH was added to a DI water–nanoparticle suspension in order to increase the pH and conductivity of the nanoparticle suspension, and a dilute solution of Na_2CO_3 and NaHCO_3 salts was added to control the ionic conductivity.

PSL nanoparticles supplied by Duke Scientific, Inc. were used in the experiments because of their ability to have a stable negative zeta potential⁴² over a wide range of pH in the aqueous solution. On the basis of the simplified Debye–Hückel approximation of the Derjaguin–Landau–Verwey–Overbeek theory, the charge on such a

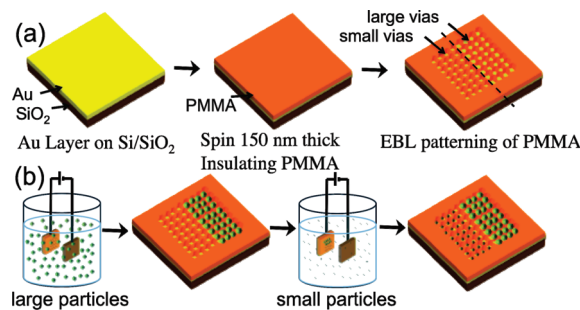


Figure 1. (a) Schematic diagram of template fabrication. (b) Schematic diagram of the sequential electrophoretic assembly process.

particle is given by^{43,44}

$$q = 4\pi r \epsilon (1 + \kappa r) \zeta \quad (1)$$

where r , ϵ , κ , and ζ are the radius of the particle, the dielectric constant of the suspension, the inverse Debye length (Debye–Hückel parameter), and the zeta potential of the particle, respectively. The pH and electrical conductivity of the nanoparticle suspension were maintained at 11 and 450 μS , respectively, throughout the experiments.

Sequential Electrophoretic Assembly. The electrophoretic assembly of nanoparticles was performed by applying a dc voltage between the topographically patterned PMMA/gold template (anode) and a gold substrate (cathode) in the nanoparticle suspension (Figure 1b). A dc power source (Keithley 2400) was used to control the magnitude of the applied voltage. The spacing between the electrodes (patterned template and gold substrate) was kept at 5 mm during the assembly process. For experimental consistency, we used a dip coater provided by KSV Instruments to control the vertical speed of the template during the insertion and removal from the suspension. The vertical speed of the electrodes was maintained at 85 mm/min. The electrostatic force acting on the negatively charged colloidal nanoparticles is directly proportional to the strength of the electric field between the electrodes and the charge of the particle. Our experiments show that nanoparticles assemble into the vias when a voltage of 2 to 3 V was applied between the electrodes for 1 to 2 min.

For the size-selective assembly of two different particle sizes, we patterned the template with arrays of two differently sized vias. Each via size was designed to be equal or slightly larger than the corresponding nanoparticle size. The sequential assembly process for sorting two different particle sizes consisted of two steps (Figure 1b). First, the larger particles were assembled into vias that were equal to or larger than the particle diameter. After the first step, the smaller vias remained empty because the larger particles did not fit into them. Then, the same template with already-assembled larger particles was submerged into another suspension to assemble the smaller nanoparticles into the smaller vias. This sequential assembly process can be used to sort more than two particle sizes by adding more via sizes and assembly steps.

RESULTS AND DISCUSSION

Sorting Efficiency. The sorting efficiency depends on the number of defects after the complete assembly process. A defect occurs when particles are not assembled in a via or if a smaller particle assembles into a larger via. Smaller particles can assemble into the larger vias if the larger via is empty or if there is enough space left next to the assembled larger particle. The sorting efficiency is defined as the ratio of the total number of vias minus defects to the total number of vias in the array.

To demonstrate the effectiveness of the assembly technique in sorting nanoparticles of two different sizes, we have performed the

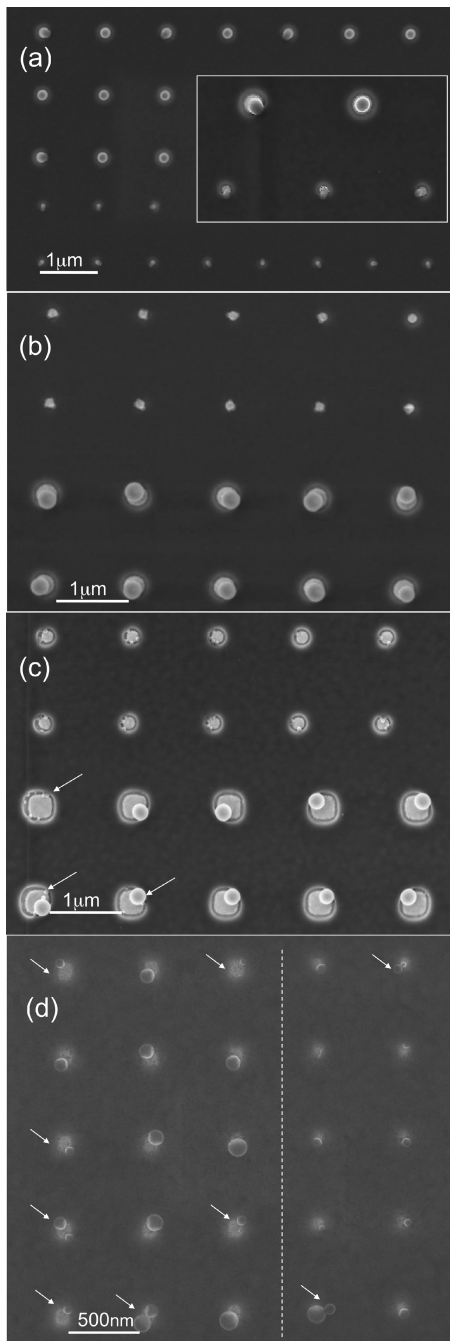


Figure 2. (a) SEM micrograph after the second stage of the sequential assembly process in which 200 and 100 nm particles were assembled into 1- μm -spaced vias with dimensions of 210 and 110 nm. (b) SEM micrograph of 200 and 50 nm PSL nanoparticles assembled in 1- μm -spaced vias with dimensions of 225 and 100 nm, respectively. (c) SEM micrograph of 200 and 50 nm PSL nanoparticles assembled in 1- μm -spaced 300 and 150 nm vias. (d) SEM micrograph demonstrating the size-selective assembly of 100 and 60 nm particles assembled in 110 and 70 nm vias separated by 500 nm.

size-selective assembly of 200–100, 200–50, and 100–60 nm particles. Figure 2a shows the sequential assembly of 200 and 100 nm PSL particles into an array of 210 and 110 nm vias. The 200 nm particles were first assembled into 210 nm vias, then the template with already-assembled 200 nm particles was inserted into 100 nm particle suspension for the electrophoretic assembly. Because

Table 1. Sorting Efficiency^a

particle size (nm)	via size (nm)	sorting efficiency (%)	standard deviation (%)
200–100	210–110	100	0
200–50	225–100	98.7	2.31
200–50	300–150	81.3	12.2
100–60	110–70	<56	

^a Summary of the sorting efficiency achieved for four different nanoparticle size/via size pairs averaged over three different experiments.

the 210 nm vias were all filled with 200 nm particles, 100 nm particles were assembled only in the 110 nm vias as shown in Figure 2a.

Figure 2b,c shows the sequential assembly of 200 and 50 nm particles in the 225–100 and 300–150 nm vias, respectively. In contrast to nondefective sorting in Figure 2a,b, the assembly of 50 nm particles in some of the 300 nm vias was observed in Figure 2c. Because the size of the vias in Figure 2c was much larger than the respective nanoparticle diameter, 50 nm particles were assembled in the empty space next to the 200 nm particles. This led to defects in the array, decreasing the sorting efficiency.

To explore the capability of a sequential size-selective technique in separating particles with sizes close to each other, the selective assembly of 100 and 60 nm was performed. An analysis of the 60 and 100 nm particle suspensions with a Malvern zetasizer showed a large overlap between the two particle size distributions. Because of the large size variation in the 100 nm particle suspension, various particle sizes besides the 100 nm particles can fill the 110 and 60 nm vias after the first assembly step. As a result, defects are generated and the sorting efficiency is decreased. Figure 2d shows the results and defects observed for the assembly of 100 and 60 nm particles into 110 and 70 nm vias. These types of defects were not observed during the sorting of 200 and 50 nm nanoparticles where there is no overlap between the size distributions of the pair (Figure 2b,c). Therefore, the size difference in selective assembly is constrained by the size distribution of the chosen particles. It is important to have nanoparticles with a narrow size distribution when size-selective assembly is performed on the particles with sizes close to each other. To conduct an assembly of nanoparticles with a size difference of less than 40 nm, the suspension can be filtered to remove the small particles (before functionalization) for each size distribution to eliminate the overlap. In this study, the problem of overlap was resolved by choosing particle sizes that do not overlap.

Table 1 summarizes the calculated sorting efficiency for the size-selective assembly experiments carried out with different via sizes and particles sizes. We evaluate the sorting efficiency of each template by considering 25 vias (a 5 × 5 array) in the middle of the array. To achieve an accurate estimation of the sorting efficiency, the arithmetic average of three experiments is presented for each of the four conditions. The results show that the sorting efficiency is higher when the particle diameter is closer to the via size. When the via size is not close to the respective particle diameter, there is enough space for the smaller particle to assemble next to the larger ones and the sorting efficiency decreases. The size variation in the particle suspension also decreases the sorting efficiency when the particles are close in size.

Effect of Voltage on Particle Detachment. We noticed that during the sequential assembly process, when a template with assembled nanoparticles was inserted into another nanoparticle suspension for assembly, many of the previously assembled

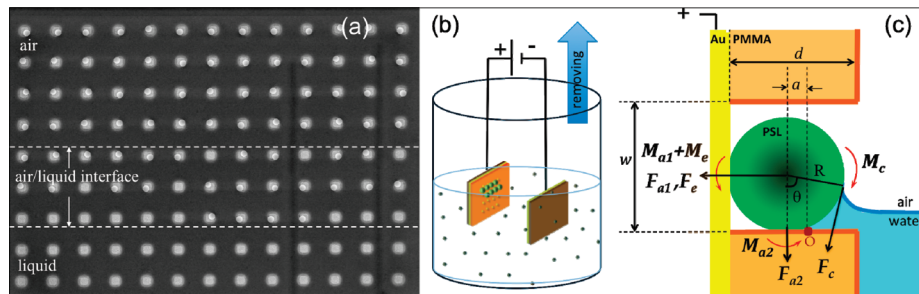


Figure 3. (a) SEM micrograph shows a patterned substrate with assembled 200 nm particles. The voltage was turned off when the substrate was half way out of the particle suspension. (b) Schematic diagram of the electrophoretic assembly setup being removed from the particle suspension; negatively charged nanoparticles are assembled on the positively charged patterned template. (c) Schematic diagram of the cross section of the patterned template showing various forces acting on the assembled nanoparticle during the insertion and removal of the template into the nanoparticle suspension. F_e is the force experienced by the particle due to the applied electric field, and F_{a1} and F_{a2} are the adhesion forces between the nanoparticle and gold substrate and nanoparticle and PMMA film, respectively. Here, a is the contact radius resulting from the adhesion-induced deformation.

nanoparticles were detached. To prevent particle detachment, the voltage was kept on while the template was withdrawn from the suspension. To demonstrate the effect of voltage on sequential assembly, we conducted a single-step assembly experiment where the voltage is kept on while the template is withdrawn from the suspension and the voltage is turned off when the template is half way out of the suspension. Figure 3a shows that the assembled 200 nm particles are detached from the 1- μm -spaced vias in the bottom part of the template, where the voltage is turned off during removal. At the instant when the voltage was turned off, the top half of the substrate (the region above the dashed lines) was already out of the suspension and therefore the particles have remained in the vias. The region between the lines is the interface of the liquid–air–substrate or the liquid level when the voltage was turned off. In the interface region, some particles were removed whereas others remained. The region below the dashed lines was submerged in the liquid suspension when the voltage was turned off. Therefore, all of the particles in this region were detached from the vias upon removal of the substrate from the liquid suspension as a result of the moment exerted on the particles by the interfacial capillary force at the liquid–air–substrate interface. To understand the effect of the capillary force on particle detachment, we consider a nanoparticle having radius R assembled into a via of width w and depth d . The moments of the forces applied to the particle about the axis of rotation O when the template with assembled nanoparticles is inserted into a suspension are illustrated schematically in Figure 3c.

The removal moment is given by

$$RM = \frac{M_c}{M_{a1} + M_{a2} + M_e}$$

where M_c and M_e are the moments due to capillary and electrostatic forces and M_{a1} and M_{a2} are the moments due to adhesion forces F_{a1} and F_{a2} . If $RM < 1$, then the particle remains adhered, but if $RM > 1$, then the particle will be removed. The moments are given by

$$M_{a1} = F_{a1}\sqrt{R^2 - a^2}; M_{a2} = F_{a2}a; M_e = F_e\sqrt{R^2 - a^2}$$

and

$$M_c = F_c f(\theta) \text{ where } \max[f(\theta)] \cong 1$$

For a PSL nanoparticle with a diameter of 100 nm assembled into a via with a depth of $d > R + a$, the capillary force is on the order of 10^{-8} N ,⁴⁵ and for $a_{\text{exp}} \approx 0.1R$,⁴⁶ the maximum moment

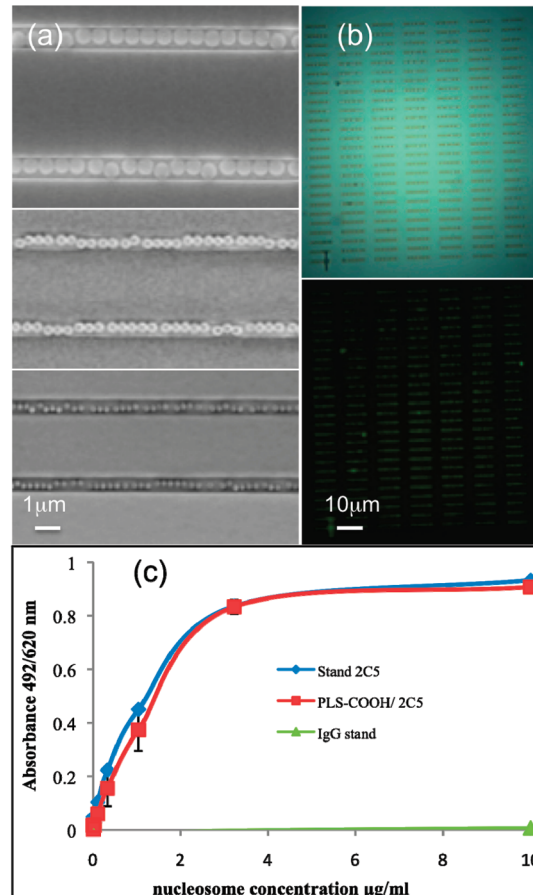


Figure 4. (a) SEM image of 500 nm PSL assembled in 550-nm-wide and 300-nm-deep trenches (top), 330 nm mAb-2C5-coated carboxylic-functionalized particles assembled in 400-nm-wide and 300-nm-deep trenches (middle), and 200 nm fluorescent nanoparticles assembled in 250-nm-wide and 150-nm-deep trenches. (b) Bright-field microscope image of 330 nm mAb-2C5-coated carboxylic-functionalized PSL particles assembled into nanotrenches for *in vitro* antigen detection (top). Fluorescence microscope image of the *in vitro* biosensor after the fluorescently tagged nucleosome is detected (bottom). (c) Indirect ELISA testing of the activity of the mAb-2C5-coated PSL beads compared to free mAb-2C5 and nonspecific IgG against the nucleosome antigen.

due to the capillary force during insertion is $M_{c,\text{max}} = 5 \times 10^{-16} \text{ J}$. The moments due to the adhesion of a PSL particle with a

diameter of 100 nm to gold and PMMA are approximately $M_{a1} = 2.03 \times 10^{-16}$ J and $M_{a2} = 3.1 \times 10^{-18}$ J, respectively. The deformation of a soft particle on a hard substrate increases the adhesion force, and this deformation typically occurs a few hours after the particles have been deposited.⁴⁷ In our process, because various stages of the sequential assembly of nanoparticles are carried out within minutes, the contribution of the deformation-induced adhesion force would be negligible and hence the actual total adhesion force would be less than 10^{-9} N. In the absence of the electric field, the moment ratio is $2.4 > 1$. This implies that the particle will be removed.

Under our experimental conditions, the charge on a 100 nm particle calculated from eq 1 is $q \approx 10^{-15}$ C and the magnitude of the local electric field applied in the vicinity of the fabricated vias is on the order of 10^7 V/m for an applied potential of 2 V between the electrodes separated by a distance of 5 mm. Therefore, the electrostatic force acting on the particle is on the order of 10^{-8} N and the moment due to this electrostatic force about O is 4.95×10^{-16} J. When the electric field is applied, the moment ratio is $0.7 < 1$ and hence the particle remains adhered to the substrate. Therefore, an electrostatic field must be applied while the template is inserted into or removed from a suspension to prevent already-assembled particles from being detached.

Nanoparticle Assembly in Trenches and Antigen Detection.

Figure 4a shows that it is possible to assemble nanoparticles electrophoretically with various sizes, functionalizations, and antibody coatings inside trenches with width and depth comparable to their size. The high density of the mAb-coated particles arranged inside trenches in a small area of a chip (Figure 4a, middle) provides a single analyte in an in vitro biosensing device. The in vitro sensors were fabricated and tested with the following procedure: Cancer-specific mAb-2CS recognizing intact nucleosome (NS)⁴⁸ on the surface of cancer cells was coated onto 330 nm carboxylic-functionalized PSL nanoparticles. The mAb-2CS-coated PSL was then assembled into trenches on the surface of a chip in order to develop an immunoassay biosensor for the detection of the NS antigen.

The activity was detected using a standard indirect enzyme-linked immunosorbent assay (ELISA) by incubating the microchip with known concentrations of fluorescently labeled NS. The chip was then imaged with a fluorescence microscope to measure the intensity of the fluorescence signal. The results show that the intensity of the fluorescence detected correlates with the NS concentration used in the experiment (Figure 4b). NS concentrations as low as $1 \mu\text{g}/\text{mL}$ were detected using this nanoparticle-based biosensor. Figure 4c shows the test results of the activity of the mAb-2CS-coated PSL beads compared to those of free mAb-2CS and nonspecific IgG against the NS antigen.

It has been shown that an *in vivo* nanoparticle-based biosensor as small as $100 \mu\text{m} \times 100 \mu\text{m}$ can be fabricated and attached to the top of $300 \mu\text{m}$ catheters utilizing a custom-built biosensor microassembly.⁴⁹ The reported *in vivo* biosensor can adopt our proposed size-selective assembly technique in order to assemble multiple nanoparticles with various mAb coatings to facilitate the multiplex *in vivo* detection of diseases.

CONCLUSIONS

We have shown that nanoparticles of different sizes can be selectively assembled into prefabricated nanostructure arrays on a template using a sequential template-directed assembly method. Polystyrene latex (PSL) nanoparticles with diameters ranging from 200 to 50 nm have been selectively assembled on different regions

on the same template. It is also shown that it is necessary to apply the electric field during the various steps of the sequential assembly process to prevent the detachment of previously assembled particles. For this directed assembly technique, the sorting efficiency depends on the particle size/via size ratio and also on the size distribution of the particles when the chosen nanoparticles are close in size. We have also shown that a high sorting efficiency is achieved when the nanoparticles are assembled in vias close to their size and when the size difference between the larger and smaller particles in the assembly sequence is larger than the width of the size distribution of the particles. This approach offers a simple, fast, repeatable method for the precise size-selective positioning of nanoelements on a large scale and in a short time.

The detection capacity of the nanoparticle-based biosensor has been tested with a single analyte system of cancer-specific mAb-2CS/nucleosome. It is shown that a nucleosome concentration of as low as $1 \mu\text{g}/\text{mL}$ can be detected. This suggests that the size-selective assembly technique may pave the way for fabricating a nanoparticle-based microbiosensor for the detection of multiple biomarkers as well as many applications where the assembly of nano building blocks with different biological or chemical functionalization is necessary. Further investigation into multiple sensing capabilities is currently ongoing.

ASSOCIATED CONTENT

S Supporting Information. SEM image of the selective assembly after the first assembly step, size distribution of the nanoparticles, and experimental demonstration of the effect of voltage on particle detachment. This material is available free of charge via the Internet at <http://pubs.acs.org>.

AUTHOR INFORMATION

Corresponding Author

*E-mail: busnaina@coe.neu.edu.

ACKNOWLEDGMENT

We are grateful for a W. M. Keck Foundation grant and a National Science Foundation Nanoscale Science and Engineering Center (NSEC) for High-Rate Nanomanufacturing grant (NSF grant no. 0425826). The experiments have been conducted at the George J. Kostas Nanoscale Technology and Manufacturing Research Center.

REFERENCES

- Ozin, G. A.; Yang, S. M. *Adv. Funct. Mater.* **2001**, *11*, 95.
- Scott, R. W. J.; Yang, S. M.; Coombs, N.; Ozin, G. A.; Williams, D. E. *Adv. Funct. Mater.* **2003**, *13*, 225.
- Cui, Y.; Bjork, M. T.; Liddle, J. A.; Sonnichsen, C.; Bousquet, B.; Alivisatos, P. A. *Nano Lett.* **2004**, *4*, 1093.
- Xia, Y.; Gates, B.; Yin, Y.; Lu, Y. *Adv. Mater.* **2000**, *12*, 693.
- Su, K. H.; Wei, Q. H.; Zhang, X.; Mock, J. J.; Smith, D. R.; Schultz, S. *Nano Lett.* **2001**, *3*, 1087.
- Kruis, F. E.; Fissan, H.; Peled, A. J. *Aerosol Sci.* **1998**, *29*, 511.
- Shipway, A.; Katz, E.; Willner, I. *ChemPhysChem* **2000**, *1*, 18–52.
- Engvall, E.; Perlmann, P. O. *Immunochemistry* **1971**, *8*, 871–875.
- Nam, J.; Thaxton, C. S.; Mirkin, C. *Science* **2003**, *301*, 1884.
- Luo, X.; Morrin, A.; Killard, A.; Smyth, M. R. *Electroanalysis* **2006**, *18*, 319.
- Brogan, K. L.; Patricia, K. N.; Jones, P. A.; Schoenfisch, M. *Anal. Chim. Acta* **2010**, *496*, 73.

- (12) Luo, X.; Morrin, A.; Killard, A. J.; Smyth, M. R. *Electroanalysis* **2006**, *18*, 319.
- (13) Zhuo, Y.; Yuan, R.; Chai, Y. Q.; Tang, D. P.; Zhang, Y.; Wang, N.; Li, X. L.; Zhu, Q. *Electrochim. Commun.* **2005**, *7*, 355.
- (14) Darbha, G.; Ray, A.; Ray, P. *ACS Nano* **2007**, *3*, 208.
- (15) Sandros, M.; Benson, D. *J. Am. Chem. Soc.* **2005**, *127*, 12198.
- (16) Zheng, G.; Patolsky, F.; Cui, Y.; Wang, W. U.; Lieber, C. M. *Nat. Biotechnol.* **2005**, *23*, 1294.
- (17) Fan, R.; Vermesh, O.; Srivastava, A.; Yen, B. K. H.; Qin, L.; Ahmad, H.; Kwong, G. A.; Liu, C.; Gould, J.; Hood, L.; Heath, J. R. *Nat. Biotechnol.* **2008**, *26*, 1373.
- (18) Hansen, J.; Wang, J.; Kawde, A.; Xiang, Y. *J. Am. Chem. Soc.* **2006**, *128*, 2228.
- (19) Yan, R.; Mestas, S.; Yuan, G.; Safaisini, R. *Lab Chip* **2009**, *9*, 2163.
- (20) Harper, J.; Polksy, R.; Wheeler, D.; Dirk, S.; Brozik, S. M. *Langmuir* **2007**, *23*, 8286.
- (21) Im, J.; Chandekar, A.; Whitten, J. *Langmuir* **2009**, *25*, 4288.
- (22) You, C.; Miranda, O.; Gider, B.; Ghosh, P. *Nat. Nanotechnol.* **2007**, *2*, 318.
- (23) Whitesides, G. M.; Grzybowski, B. *Science* **2002**, *295*, 2418.
- (24) Hoogenboom, J. P.; Langen-Suurling, A. K. V.; Romijn, J.; Blaaderen, A. V. *Phys. Rev. Lett.* **2003**, *90*, 38301.
- (25) Ye, Y. H.; Badilescu, S.; Truong, V.; Rochon, P.; Natansohn, A. *Appl. Phys. Lett.* **2001**, *79*, 872.
- (26) Maury, P.; Escalante, M.; Reinhoudt, D. N.; Huskens, J. *Adv. Mater.* **2005**, *17*, 2718.
- (27) Velev, O. D.; Bhatt, K. H. *Soft Matter* **2006**, *2*, 738.
- (28) Yilmaz, C.; Tae-Hoon Kim, T. H.; Somu, S.; Busnaina, A. A. *IEEE Trans. Nanotechnol.* **2010**, *9*, 653.
- (29) X. Xiong, X.; Makaram, P.; Busnaina, A.; Bakhtari, K.; Somu, S.; McGruer, N.; Park, J. *Appl. Phys. Lett.* **2006**, *89*, 193108–1.
- (30) Fan, F.; Stebe, K. J. *Langmuir* **2005**, *21*, 1149.
- (31) Plutowski, U.; Jester, S. S.; Lenhart, S.; Kappes, M. M.; Richert, C. *Adv. Mater.* **2007**, *19*, 1951.
- (32) Gotesman, G.; Naaman, R. *Langmuir* **2008**, *24*, 5981.
- (33) Lee, I.; Zheng, H.; Rubner, M. F.; Hammond, P. T. *Adv. Mater.* **2002**, *14*, 569.
- (34) Cha, N. G.; Echegoyen, Y.; Kim, T. H.; Park, J. G.; Busnaina, A. A. *Langmuir* **2009**, *25*, 11382.
- (35) Yin, Y. D.; Xia, Y. N. *Adv. Mater.* **2001**, *13*, 267.
- (36) Xia, Y. N.; Yin, Y. D.; Lu, Y.; McLellan, J. *Adv. Funct. Mater.* **2003**, *13*, 907–918.
- (37) Varghese, B.; Cheong, F. C.; Sindhu, S.; Yu, T.; Lim, C.; Valiyaveettil, S.; Sow, C. *Langmuir* **2006**, *22*, 8248.
- (38) Yin, Y. D.; Lu, Y.; Gates, B.; Xia, Y. N. *J. Am. Chem. Soc.* **2001**, *123*, 8718–8729.
- (39) Kuemin, C.; Huckstadt, K. C.; Lörtscher, E.; Rey, A.; Decker, A.; Spencer, N. D.; Wolf, H. *Adv. Mater.* **2010**, *22*, 2804.
- (40) Rycenga, M.; Camargo, P. H. C.; Xia, Y. *Soft Matter* **2009**, *5*, 1129.
- (41) Fan, F.; Stebe, K. J. *Langmuir* **2004**, *20*, 3062–3067.
- (42) Lin, H. Ph.D. Dissertation, Clarkson University, Potsdam, NY, 2001.
- (43) Xiong, X. Ph.D. Dissertation, Northeastern University, Boston, MA, 2006.
- (44) Bakhtari, K. Ph.D. Dissertation, Northeastern University, Boston, MA, 2006.
- (45) Israelachvili, J. N. *Intermolecular and Surface Forces*, 2nd ed.; Academic Press: New York, 1992.
- (46) Hu, S. Ph.D. Dissertation, Northeastern University, Boston, MA, 2006.
- (47) Krishnan, S.; Busnaina, A. A.; Rimai, D. S.; DeMejo, D. P. *J. Adhes. Sci. Technol.* **1994**, *8*, 1357.
- (48) Torchilin, V. P.; Iakoubov, L. Z.; Estrov, Z. *Trends Immunol.* **2001**, *22*, 424.
- (49) Malima, A.; Busnaina, A.; Somu, S. *Proc. ASME (IDETC/CIE2009)* **2009**, 485.